

# R<sup>3</sup>-Avatar: Record and Retrieve Temporal Codebook for Reconstructing Photorealistic Human Avatars

Yifan Zhan<sup>1,2\*</sup> Wangze Xu<sup>1</sup> Qingtian Zhu<sup>2</sup> Muyao Niu<sup>2</sup> Mingze Ma<sup>2</sup> Yifei Liu<sup>1,3</sup>  
 Zhihang Zhong<sup>1†</sup> Xiao Sun<sup>1†</sup> Yinqiang Zheng<sup>2</sup>

<sup>1</sup>Shanghai Artificial Intelligence Laboratory

<sup>2</sup>The University of Tokyo

<sup>3</sup>Beihang University

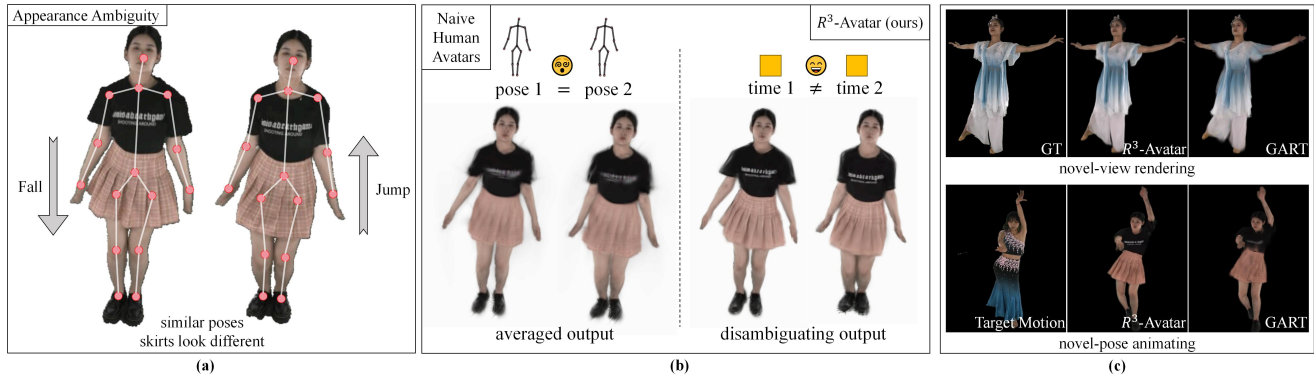


Figure 1. (a) A case to show appearance ambiguity. The skirts of a same posed human look different due to different motion patterns (fall and jump). (b) Our disambiguating “record-retrieve-reconstruct” strategy compared to the naive pose-input training pipeline, which is easily exposed to appearance ambiguity. (c) A glimpse of the results of the rendering and animation.

## Abstract

We present R<sup>3</sup>-Avatar, incorporating a temporal codebook, to overcome the inability of human avatars to be both animatable and of high-fidelity rendering quality. Existing video-based reconstruction of 3D human avatars either focuses solely on rendering, lacking animation support, or learns a pose-appearance mapping for animating, which degrades under limited training poses or complex clothing. In this paper, we adopt a “record-retrieve-reconstruct” strategy that ensures high-quality rendering from novel views while mitigating degradation in novel poses. Specifically, disambiguating timestamps record temporal appearance variations in a codebook, ensuring high-fidelity novel-view rendering, while novel poses retrieve corresponding timestamps by matching the most similar training poses for augmented appearance. Our R<sup>3</sup>-Avatar outperforms cutting-edge video-based human avatar reconstruction, particularly in overcoming visual quality degradation in extreme scenarios with limited training human poses and complex clothing. Code will be available at <https://github.com/Yifever20002/R3Avatars>.

\*This work was done during the author’s internship at the Shanghai Artificial Intelligence Laboratory. † denotes co-corresponding authors.

## 1. Introduction

The emergence of 3D Gaussian Splatting [32] (3DGS) catches our attention once again to the reconstruction of digital human avatars. Taking advantage of the rendering efficiency of 3DGS and its exceptional performance in novel view synthesis, recovering 3D avatars from human videos with gaussian representations [21, 35, 40, 49, 55] outperforms earlier Neural Radiance Fields [45] (NeRF)-based neural rendering methods [39, 53, 68, 71], raising expectations for enhanced rendering and animation quality in graphics and VR/AR technologies.

Existing modelings of digital human, however, struggle to escape the curse of being unable to balance both animating and rendering. To achieve animation, human gaussians are constrained by pre-extracted human poses [21] or pose embeddings (e.g., a motion-aware map [49]) to learn human appearance across different frames. Fig. 1 (a) shows a typical one-to-many mapping, as noted by Chen et al. [6], where similar poses are mapped to different appearances, thus limiting the modeling capacity of human gaussians. Such ambiguities become more pronounced as the complexity of clothing increases. Other rendering-based methods [28, 29, 41, 77, 84, 87] reconstruct per-frame human appearance without rigging a skeleton, limiting their ability

to animate and perform other downstream tasks.

Since pose-appearance mapping is difficult to learn, could there be a “mode-seeking” approach that bypasses this learning process by first storing the appearance from the training set and then using the pose as a key to retrieving during animation? Accordingly, a “record-retrieve-reconstruct” strategy is implemented in this paper, where disambiguating recording of a temporal codebook enhances novel-view rendering, which is later retrieved by human poses to augment the appearance during animation.

For training during the recording phase, we maintain an explicit temporal codebook conditioned on timestamps to remember the variations of human appearance exploited in the provided video sequence. Since human clothing exhibits non-rigid motions, we define the codebook in the T-pose space to decouple it from rigid motion, with the latter represented by the Linear Blend Skinning [44] (LBS) model. Given the challenges of using a deformation field [55] to represent inter-frame motion of human clothing, we design a 4D gaussian decoder that directly outputs gaussian attributes in the canonical space for each timestamp. In this way, the rendering at novel views could be guaranteed.

To tackle the lack of temporal information when performing animation under novel pose sequences, we propose a retrieving algorithm to determine the timestamps according to the similarity between novel poses and training poses. However, directly matching the human poses of the whole body will fail due to limited matching samples. To overcome this, we partition the human body, allowing different body parts to act asynchronously. Then, we leverage pose sequences [6] to consider motion direction for more accurate matching. To ensure visual coherence in animation, we further introduce a smoothing process. The above components collectively form our retrieving algorithm.

We evaluate our method on multi-view datasets of humans with complex clothing, including DNA-Rendering dataset [7] and HiFi4G dataset [29]. To validate that our representation does not degrade in simpler clothing scenarios, we additionally compared it with the ZJU\_MoCap dataset [52] and MVHumanNet dataset [72]. To summarize, our contributions are three-fold as follows:

- 1) a disambiguating training pipeline of human gaussians conditioned on timestamps, with a temporal codebook and a 4D gaussian decoder for efficient human appearance recording;
- 2) a retrieving algorithm to obtain corresponding timestamps for novel poses, involving body-part decoupling, pose sequence matching, and appearance smoothing;
- 3) state-of-the-art performance in both rendering and animating on datasets with diverse clothing complexities, compared to cutting-edge reconstructions of video-based 3D human avatars.

## 2. Related Work

### 2.1. SMPL(-X) and Regression-based Human Avatars

Most digital human works are built upon skinned vertex-based models such as SMPL(-X) [44, 51], which parameterizes the human body mesh as customized shape and motion-related joint poses. The human body under different poses is constructed by linearly blending the mesh in the canonical space with the current joint poses. This process is known as Linear Blend Skinning (LBS). By the aid of the SMPL(-X) model and data-driven approaches, recovering the texture of a 3D human from images [16, 17, 23, 57, 58, 73, 74, 85] and videos [2, 11, 14, 15, 75] becomes possible. However, SMPL is unable to model the motion of clothing, leading some works [4, 46] to focus on clothing reconstruction.

### 2.2. Neural Animatable Human Avatars

The emergence of NeRF [45] has provided a new approach for 3D human avatar reconstruction. Many NeRF-based methods backward-warp the human body to construct a neural radiance field of the human body in the canonical T-pose, leveraging human poses [12, 26, 27, 33, 37, 39, 52, 54, 60–62, 68, 71, 79, 80, 86] or motion-aware maps [10, 42, 83]. Recent advancements in 3DGS [32] have further boosted the quality of neural rendering, leading to a surge in digital human research. However, the rendering of clothing, as an important part of human avatars, has not been fully addressed. Some human gaussian works [21, 25, 31, 34, 43, 47, 49, 50, 59] ignore non-rigid appearance modeling while others [35, 40, 47, 55] formulate the non-rigid part with human pose condition, not managing to escape from appearance ambiguities. Generative methods have been introduced to enhance the rendering quality from unseen views [70]. We notice that frame index is used in [36] to alleviate such ambiguity trivially, incapable of accurately learning the variations in appearance and animating. Pose sequence embedding proposed by [6, 76] serves as a disambiguating condition for appearance learning, while still suffering from the tricky selection of sequence length and steps, which is critical for training results. Our 4D gaussian decoder draws inspiration from [20, 34, 89], and further incorporates a temporal codebook to acquire human gaussian attributes for each timestamp.

### 2.3. Human Volume Rendering

Rendering-based human avatars focus on recovering 3D human bodies from images or videos without the requirement for animation. A class of methods [24, 28, 29, 41, 77, 84, 87] employs multi-view image-based rendering strategies, using reference views to enhance the rendering quality from source views. Other methods [1, 3, 5, 19, 22, 48, 63, 64, 81] aim to recover 3D textured humans from a single

image with diffusion models. Svitov et al. [64] allow for simple animation, but limited to tight-fitting garments conforming to the SMPL geometry. Guo et al. [13] and Tan et al. [65] can recover complex clothing from a monocular video without performing animation. It is worth noting that the concept of a codebook [8, 67, 88], or look-up table [30, 38] (LUT), has been used to store information during training, enabling faster and more accurate inference.

### 3. Preliminaries

#### 3.1. SMPL(-X)

The Skinned Multi-Person Linear (SMPL) [44] model consists of human shape and pose parameters as well as per-vertex blending weights, which is learned from thousands of 3D human scans. The canonical human mesh template  $\mathbf{x}_c$  can be transformed into  $\mathbf{x}_o$  in the observation space through LBS process, following

$$\mathbf{x}_o = \sum_{k=1}^K \omega_k(\mathbf{x}_c)(R_k(\boldsymbol{\theta})\mathbf{x}_c + t_k(\mathbf{j}, \boldsymbol{\beta})), \quad (1)$$

where  $K$  is the number of joints,  $\omega_k$  is the per-joint linear blending weight,  $R_k$  is the per-joint global rotation calculated by local human pose  $\boldsymbol{\theta}$  and  $t_k$  is the per-joint global translation calculated by joint position  $\mathbf{j}$  and human shape  $\boldsymbol{\beta}$ . Subsequent works extend the SMPL skeleton to include the hands [56] and expressive faces [51]. For human gaussian rendering, SMPL vertices provide a good gaussian initialization and blending weights. Nevertheless, clothed humans do not fully conform to the SMPL geometry, requiring the optimization of LBS weights. Furthermore, recovering complex clothing through pose-based linear blending presents big challenges.

#### 3.2. 3D Gaussian Splatting

3DGS [32] represents 3D scenes by explicitly defining optimizable gaussian units. Specifically, each gaussian unit can be defined as

$$G(\mathbf{x}) = \frac{1}{(2\pi)^{\frac{3}{2}} |\boldsymbol{\Sigma}|^{\frac{1}{2}}} e^{-\frac{1}{2}(\mathbf{x}-\boldsymbol{\mu})^T \boldsymbol{\Sigma}^{-1}(\mathbf{x}-\boldsymbol{\mu})}, \quad (2)$$

where  $\boldsymbol{\mu}$  is the gaussian center, and  $\boldsymbol{\Sigma}$  is the 3D covariance matrix, which will be further decomposed into learnable rotation  $\mathbf{R}$  and scale  $\mathbf{S}$ . Other properties include gaussian color  $c$  and opacity  $\alpha$ .

During the tile-based rendering, 3D gaussians are projected onto 2D, and the final screen color is determined based on  $\alpha$ -blending following

$$C = \sum_{i \in N} c_i \alpha_i \prod_{j=1}^{i-1} (1 - \alpha_j). \quad (3)$$

The gaussian properties will be optimized with image supervision. An adaptive density control strategy is applied

to the number of 3D gaussians through splitting and pruning. Furthermore, opacity is periodically reset to remove non-salient gaussians.

#### 3.3. Rigid Body Transformation

The canonical 3DGS attributes ( $\mathbf{x}_c, \alpha, \mathbf{q}_c, \mathbf{s}$ , sh) can be warped to the observation space using the LBS method. Based on Eq. (1), the Euler transformation from the canonical space to the observation space is  $T = \sum_{k=1}^K \omega_k T_k$ ,  $T_k = \begin{bmatrix} R_k & t_k \\ 0 & 1 \end{bmatrix}$ .  $T$  is applied to the gaussian geometric properties  $\mathbf{x}_c$  and  $\mathbf{q}_c$  according to

$$\mathbf{x}_o = T\mathbf{x}_c, \quad \mathbf{R}_o = T\mathbf{R}_c, \quad (4)$$

where  $R$  is the matrix form of rotation  $q$ .

### 4. Methods

In this section, we will provide a detailed description of our ‘‘record-retrieve-reconstruct’’ strategy. We first explain our training framework, where the time-related non-rigid appearance is *recorded* by a hex-plane encoder and a 4D gaussian decoder, and the rigid spatial transformation is achieved through the LBS process. Next, we will elaborate on our *retrieving* strategy for both novel-view rendering and novel-pose animation, ensuring the accurate recovery of appearance while maintaining temporal smoothness during motion. Please refer to Fig. 2 for an overview of the entire pipeline.

#### 4.1. Hex-plane Spatio-temporal Encoder

We begin with a set of 3D points  $\mathbf{x}_c \in \mathcal{R}^3$  defined in the canonical space and explore how to obtain the 3D gaussians in the observation space at each time frame  $t \in \mathcal{R}^1$ . For an efficient encoding process, we adopt a hex-plane spatio-temporal encoder [9] with 6 orthogonal feature planes each in shape  $H \times W \times C$ , noted as ( $\mathbf{P}_{xy}, \mathbf{P}_{xz}, \mathbf{P}_{yz}, \mathbf{P}_{xt}, \mathbf{P}_{yt}, \mathbf{P}_{zt}$ ). Given a 4D input ( $\mathbf{x}_c, t$ ), each feature plane is queried and bilinearly interpolated to obtain ( $\mathbf{f}_{xy}, \mathbf{f}_{xz}, \mathbf{f}_{yz}, \mathbf{f}_{xt}, \mathbf{f}_{yt}, \mathbf{f}_{zt}$ ), which will be multiplied to get the spatio-temporal feature  $\mathbf{f} \in \mathcal{R}^C$ . We expect the spatial planes ( $\mathbf{P}_{xy}, \mathbf{P}_{xz}, \mathbf{P}_{yz}$ ) to record the canonical static information, and the temporal planes ( $\mathbf{P}_{xt}, \mathbf{P}_{yt}, \mathbf{P}_{zt}$ ) to record the appearance variations caused by clothing at different time.

#### 4.2. 4D Gaussian Decoder

The 4D gaussian decoder aims to recover 3D gaussians for each time in canonical space from spatio-temporal feature  $\mathbf{f}$ . We implement it through a simple yet efficient Multilayer Perceptron (MLP), whose input is  $\mathbf{f}$  and the corresponding output is the canonical gaussian attributes for the current frame. Our 4D gaussian decoder follows

$$(\Delta\mathbf{x}_c, \alpha, \mathbf{q}_c, \mathbf{s}) = \Phi_{gd}(\mathbf{f}). \quad (5)$$

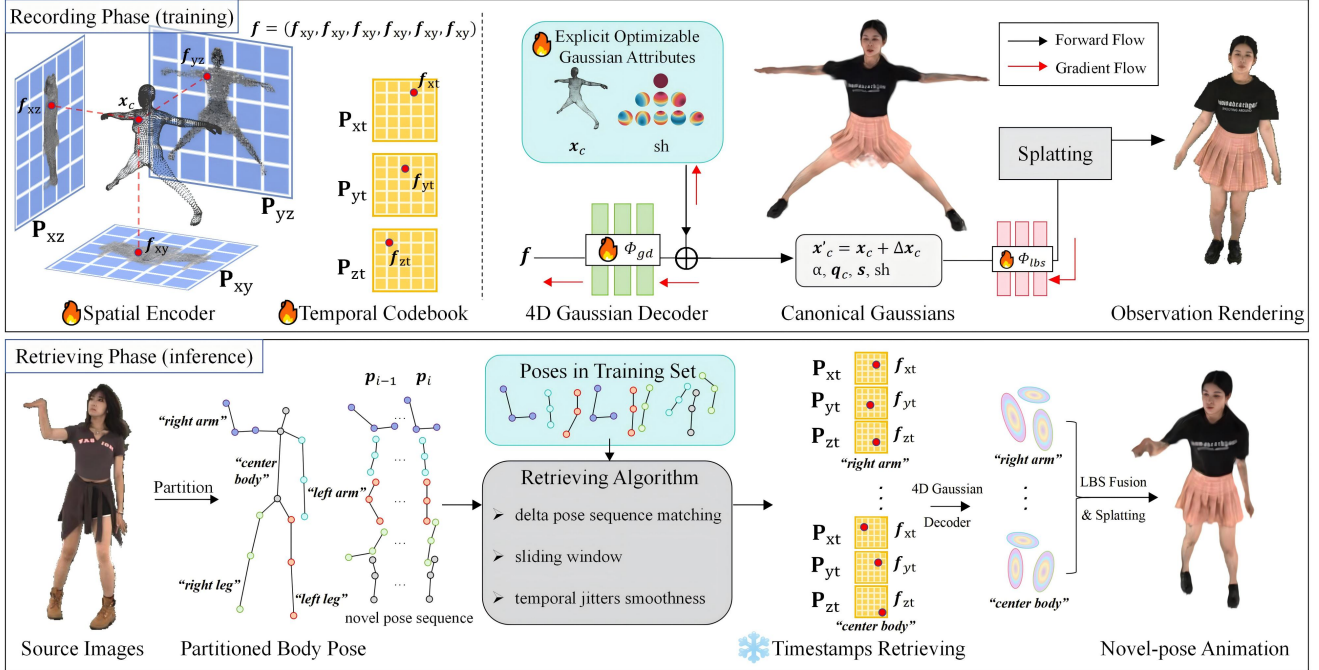


Figure 2. The pipeline of  $R^3$ -Avatar. In the “recording phase” (Sec. 4.1 and Sec. 4.2), a temporal codebook is used to capture human appearance variations over time. In the “retrieving phase” (Sec. 4.3), retrieving the temporal codebook enables high-fidelity novel-view rendering and novel-pose animation.

The canonical gaussian attributes include per-vertex offset  $\Delta \mathbf{x}_c \in \mathcal{R}^3$ , opacity  $\alpha \in \mathcal{R}^1$ , anisotropic covariance (decomposed into quaternion-represented rotation  $\mathbf{q}_c \in \mathcal{R}^4$ , and scale  $s \in \mathcal{R}^3$ ).

Note that some researches [20, 34, 47, 70, 89] also use gaussian decoders to decode gaussian attributes from MLPs. Here, we discuss the differences in the designs. Non-rigid motions are not modeled in [34], whose decoder assumes a static canonical space. Although pose-dependent non-rigid deformation is considered in [20, 47, 70, 89], the appearance ambiguity between human poses and clothing still hinders the decoder’s learning capacity. In contrast, our decoder adopts a human pose-independent 4D input, enabling disambiguating learning of appearance variations.

Another difference is that most gaussian decoders [20, 47, 70, 89] assume  $\mathbf{q}_c = [1, 0, 0, 0]$  and  $\alpha = 1$ , and do not perform adaptive density control [32] for geometry regularization. This works well for simple clothing, but experiments show that our design performs better when dealing with complex clothing. Specifically, we allow  $\mathbf{q}_c$  and  $\alpha$  to be learned freely, and permit the adaptive pruning of  $\mathbf{x}_c$ . Since color is not spatially continuous, we empirically find that learning spherical harmonics coefficients (sh) through per-gaussian optimization results better. After obtaining the canonical 3DGS attributes ( $\mathbf{x}'_c = \mathbf{x}_c + \Delta \mathbf{x}_c, \alpha, \mathbf{q}_c, s, sh$ ), we follow Sec. 3.3 to warp gaussians to the observation space. The entire framework from Sec. 4.1 to Sec. 4.2 is optimized by the loss towards the rendered 3D gaussian at-

tributes in the observation space ( $\mathbf{x}_o, \alpha, \mathbf{q}_o, s, sh$ ).

### 4.3. Appearance Retrieving for Rendering

The retrieving for novel-view rendering is simple as we already have the corresponding timestamps for novel-view images in place, thanks to multi-view synchronized capturing system. In this section, we put up with a retrieving algorithm to handle animation for time-embedded human avatars. Although our recording strategy can accurately capture the appearance in the training set, the animation ability under novel human poses are partly sacrificed as the timestamps for novel poses remain unknown.

A straightforward approach is to compare the similarity between the current novel pose  $\mathbf{p}_i$  and all possible poses  $\mathbf{p}^t$  in the training set  $\mathbf{P}^t$ , and to pick the timestamp of the frame with the most similar pose. In practice, however, it is difficult to find a sufficiently close match of whole body pose (e.g., the matched pose may be similar overall, but with opposite arm movements). Therefore, we first partition the body into 5 parts (namely center body  $\mathbf{p}_{cb}$ , left leg  $\mathbf{p}_{ll}$ , left arm  $\mathbf{p}_{la}$ , right leg  $\mathbf{p}_{rl}$ , right arm  $\mathbf{p}_{ra}$ ), assuming that the movements among these parts could be relatively independent. Now the matching samples are enriched and different parts can be retrieved with different timestamps. In the following explanation,  $\mathbf{p}_i$  will stand for per-part poses.

However, naive nearest-neighbor searching for each frame does not consider temporal smoothness, resulting in temporal jitters in the animation (i.e., the timestamps re-

---

**Algorithm 1** Retrieving Algorithm

---

**Require:**Novel delta pose  $S_{\Delta p}^N$ ,Training delta pose set  $\mathcal{S} = \{S_{\Delta p_1}, \dots, S_{\Delta p_t}, \dots\}$ .**Ensure:**To  $S_{\Delta p}^N$ , the closest  $S_{\Delta p_t}$  in  $\mathcal{S}$  and its timestamp  $t$ . $d_i = \|S_{\Delta p_i} - S_{\Delta p}^N\|_2$ , $\mathcal{S}_{\text{top}k} = \{S_{\Delta p_{(1)}}, \dots, S_{\Delta p_{(k)}}\}$ ,  $d_{(1)} \leq \dots \leq d_{(k)}$ .**if** no historical retrieving  $t_h$  **then** $t \leftarrow \text{index}(\mathcal{S}_{\text{top}k}[0])$ , $t_h \leftarrow t$ .**else**Define sliding window size  $W$ , $\mathcal{S}_{\text{valid}} = \{S_{\Delta p_{(i)}}\}$  where  $|\text{index}(\mathcal{S}_{\text{top}k}[i]) - t_h| < W$ .**if**  $|\mathcal{S}_{\text{valid}}| > 2$  **then** $t_1 \leftarrow \text{index}(\mathcal{S}_{\text{valid}}[0])$ , $t_2 \leftarrow \text{index}(\mathcal{S}_{\text{valid}}[1])$ , $t \leftarrow \frac{d_{(2)}}{d_{(1)}+d_{(2)}}t_1 + \frac{d_{(1)}}{d_{(1)}+d_{(2)}}t_2$ , $t_h \leftarrow t$ .**else if**  $|\mathcal{S}_{\text{valid}}| = 1$  **then** $t \leftarrow \text{index}(\mathcal{S}_{\text{valid}}[0])$ , $t_h \leftarrow t$ .**else** $t \leftarrow \text{index}(\mathcal{S}_{\text{top}k}[0])$ , $t_h \leftarrow t$ ,

Record a temporal jitter.

**end if****end if****return**  $t$ 

---

trieved for adjacent novel poses are far apart in the training set). To alleviate this, we first concatenate the  $\mathbf{p}_i$  with delta pose sequence [6] to form  $S_{\Delta p_i} = \{\Delta \mathbf{p}_{i-1}, \Delta \mathbf{p}_i, \mathbf{p}_i\}$  ( $\Delta \mathbf{p}_i = \delta(\mathbf{p}_i, \mathbf{p}_{i-1})$ ) to ensure that the motion direction is also considered during matching.

Furthermore, we set a sliding window to narrow down the candidates and to ensure that the next novel pose will prioritize timestamps near the time of the previous novel pose. If the number of valid timestamps within the sliding window is greater than 1, we weight the 2 most similar timestamps by the respective similarity (inversely proportional to the L2 distance between poses) to obtain a more accurate retrieval time. If there is only 1 valid timestamp within the sliding window, it will be selected directly.

In extreme cases where the input novel pose completely deviates from the training set distribution, we average the temporal features before and after the timestamps of these potential jitters to maintain the smoothness. The entire retrieving algorithm can be referenced Algorithm 1. We will thoroughly discuss the effectiveness of these modules and the ablation results in the supplemental materials.

## 5. Experiments

### 5.1. Dataset

Experiments are conducted on multi-view captured human datasets with complex clothing, namely DNA-Rendering dataset [7] and HiFi4G dataset [29]. For DNA-Rendering dataset, we select 24 surrounding views for training and 6 novel surrounding views for testing. 7 sequences (0010\_03, 0012\_03, 0019\_10, 0024\_05, 0051\_09, 0172\_05, 0188\_02) are considered, each containing frame [0,100) for training frames and [110,150) for novel human poses. For HiFi4G dataset, we select 17 surrounding views for training and 11 novel surrounding views for testing. 2 sequences (4K\_Actor1\_Greeting, 4K\_Actor2\_Dancing) are considered, each containing frame [0,140) for training frames and [150,200) for novel human poses.

We also work on two multi-view human datasets with simpler clothing, namely ZJU\_MoCap dataset [52] and MVHumanNet dataset [72] to see whether the proposed method will cause degradation. For ZJU\_MoCap dataset, we select 8 surrounding views for training and 15 novel surrounding views for testing. 6 sequences (377, 386, 387, 392, 393, 394) are considered, each containing frame [0,300) for training frames and [300,500) for novel human poses. For MVHumanNet dataset, we select 22 surrounding views for training and 9 novel surrounding views for testing. 4 sequences (100003, 100009, 100022, 100025) are considered, each containing frame [0,150) for training frames (take one frame every five frames) and [150,300) for novel human poses.

### 5.2. Baselines and Metrics

We compare with 4DGS [78] to validate that incorporating human modeling is meaningful for reconstruction of human avatars under sparse views. For human gaussian methods, we compare most cutting-edge methods including GART [35] and SplattingAvatar [59]. We also compare pose sequence embedding-based method [6] to show that our “record-retrieve-reconstruct” approach is better in dealing with appearance ambiguity. Yet not fully within the scope of our paper, we will also compare our rendering quality with non-animatable human rendering methods [41, 87] and some methods [65, 70] for recovering unseen views by incorporating priors in monocular setups, in the supplemental materials.

For novel-view rendering, we report three key metrics: peak signal-to-noise ratio (PSNR), structural similarity index measure (SSIM) [69], and learned perceptual image patch similarity (LPIPS) [82]. For novel-pose animating, we also report Frchet Inception Distance score (FID) [18]. We encourage the readers to watch the supplemental video to gain a more intuitive understanding of the animation.

Method	DNA-Rendering			HiFi4G			ZJU_MoCap			MVHumanNet		
	PSNR $\uparrow$	SSIM $\uparrow$	LPIPS $\downarrow$	PSNR $\uparrow$	SSIM $\uparrow$	LPIPS $\downarrow$	PSNR $\uparrow$	SSIM $\uparrow$	LPIPS $\downarrow$	PSNR $\uparrow$	SSIM $\uparrow$	LPIPS $\downarrow$
4DGS [78]	20.27	0.900	87.8	15.43	0.913	114.2	22.98	0.874	131.0	21.66	0.916	87.3
Dyco [6]	28.06	0.959	32.6	27.36	0.968	30.2	33.77	0.972	27.0	31.47	0.973	19.2
GART [35]	29.62	0.963	34.5	29.99	0.973	28.9	33.61	0.972	24.2	32.42	0.975	18.8
SplattingAvatar [59]	28.83	0.961	34.0	27.73	0.969	28.9	33.06	0.971	21.3	31.83	0.975	18.2
$R^3$ -Avatar (ours)	32.43	0.974	25.2	32.18	0.983	20.7	34.64	0.976	22.5	34.24	0.982	14.7

Table 1. Per-dataset quantitative comparisons on novel-view rendering. We color each result as **best**, **second best** and **third best**. LPIPS is  $1000\times$ .



Figure 3. Novel-view rendering of our method and other baselines. We compare on DNA-Rendering dataset [7] (first, second rows), ZJU\_MoCap dataset [52] (third row) and MVHumanNet dataset [72] (last row) here.

### 5.3. Comparison of Rendering and Animating

**Novel-view rendering.** In Fig. 3, Fig. 5 and Tab. 1 we display results on novel-view rendering of our methods and compared baselines. Our method achieves high-fidelity rendering results in both complex garments (first, second rows) and tight-fitting clothing (third, last rows) cases. Please refer to the supplemental video for better visualization.

**Novel-pose animating.** In Fig. 4 and Tab. 2 we show results on novel-pose animating of our methods and compared baselines. Our method maintains strong animating performance, especially when handling complex geometry and textures. To clarify, novel poses presented here belong to “in-distribution” novel poses with ground truths, as they are clipped from the same video of the training avatar (see Sec. 5.1 for detail split).

### 5.4. Ablation Studies

**The architecture of recording phase.** We design an efficient training pipeline for recording temporally varying appearance. From Tab. 3 and Fig. 6, we observe a decline in metrics when ablating individual components. Specifically, we test by replacing hex-plane encoder with positional encoding [45, 66] P.E.  $(\mathbf{x}, t)$  (w/o hex-plane), using 4d gaussian decoder to decode spherical harmonics coefficients (decoded sh), fixing rotations (fixed  $\mathbf{q}_c$ ), not decoding  $\Delta\mathbf{x}$  (w/o  $\Delta\mathbf{x}$ ), not applying adaptive density control [32] (w/o a.d.) and implementing above all (None). Among them, (w/o hex-plane) results in the most significant degradation and (decoded sh, fixed  $\mathbf{q}_c$ , w/o  $\Delta\mathbf{x}$ , w/o a.d.) lead to varying degrees of losing detail and blurring. Finally, the complete removing of these components makes the human avatar entirely inaccessible.

Method	DNA-Rendering				MVHumanNet			
	PSNR $\uparrow$	SSIM $\uparrow$	LPIPS $\downarrow$	FID $\downarrow$	PSNR $\uparrow$	SSIM $\uparrow$	LPIPS $\downarrow$	FID $\downarrow$
Dyco [6]	25.00	0.943	48.5	3.90	26.93	0.952	34.5	16.65
GART [35]	24.26	0.941	49.6	4.25	26.78	0.951	34.6	17.66
SplatingAvatar [59]	24.43	0.943	49.4	4.28	26.87	0.950	33.9	17.53
$R^3$ -Avatar (ours)	25.21	0.945	47.2	3.39	28.21	0.959	30.6	13.39

Table 2. Per-dataset quantitative comparisons on novel-pose animating. We color each result as **best**, **second best** and **third best**. LPIPS is  $1000\times$ .

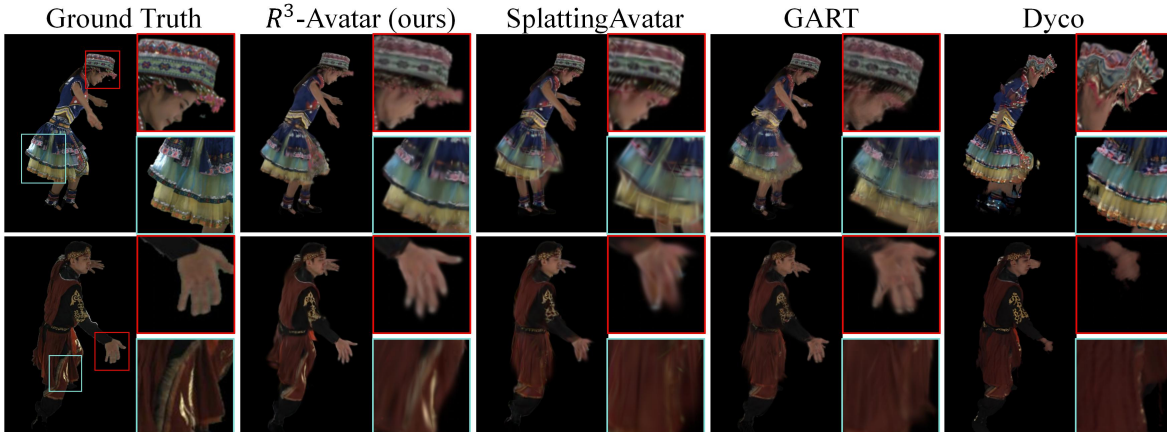


Figure 4. Novel-pose animating of our method and other baselines on DNA-Rendering dataset [7].

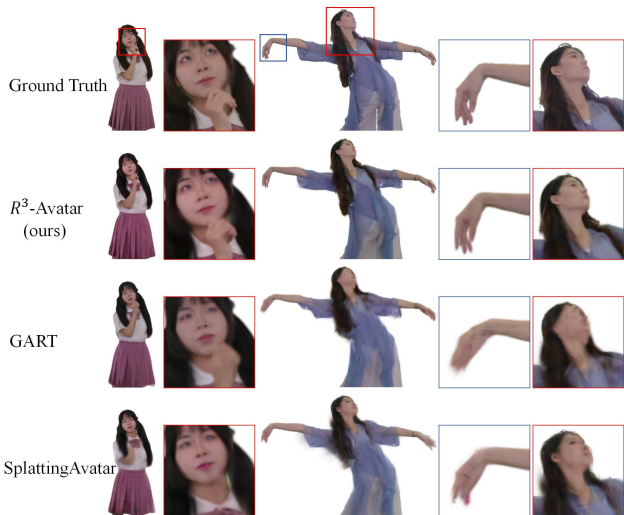


Figure 5. Novel-view rendering on HiFi4G dataset [29].

**Design of retrieving algorithm.** Our retrieving algorithm is designed to provide high-fidelity and smooth animation. To ablate, we consider not partitioning human body (w/o b.p.), not introducing sliding window (w/o s.w.), not weighting valid timestamps by their similarity (w/o w.t.) and ignoring temporal jitters smoothness (w/o t.s.).

In Fig. 7, we take “dna\_0051\_09” as an example to illustrate the impact of different designs on overall retrieving. The horizontal axis represents the index of the delta pose sequence  $S_{\Delta p}^N$  ranging from 110 to 150, while the vertical

Component	PSNR $\uparrow$	SSIM $\uparrow$	LPIPS $\downarrow$
None	29.13	0.958	53.0
w/o a.d.	32.05	0.972	30.1
w/o $\Delta x$	31.91	0.971	31.9
fixed $q_c$	32.27	0.973	28.5
decoded sh	32.06	0.973	27.0
w/o hex-plane	30.46	0.966	36.8
Full	<b>32.43</b>	<b>0.974</b>	<b>25.2</b>

Table 3. Ablations on the architecture of recording phase on DNA-Rendering dataset [7]. LPIPS is  $1000\times$ .

axis denotes the retrieved timestamps in training delta pose set  $\mathcal{S}$ . In (a), as there is no body parts, the whole body joints follow inaccurate identical retrieved timestamps, which also results in drastic temporal jitters ①. In (b), although we allow free retrieving for different body parts, the absence of a sliding window to optimize continuity of the novel appearance still leads to frequent temporal jitters. In (c), since the retrieved timestamp can only be selected from discrete training timestamps, it fails to leverage the interpolability of the temporal codebook, compromising the smoothness of the output. In (d), although smoothness is ensured, the occurrence of out-of-distribution poses still gives rise to temporal jitters, such as ②.

In Fig. 8, we demonstrate the effectiveness of temporal jitters smoothness. If there is no smoothness (row 1) at frame 126 where temporal jitters happen, the appearance undergoes drastic changes, whereas with temporal smoothness (row 2), it transitions smoothly.



Figure 6. Ablations on the architecture of recording phase.

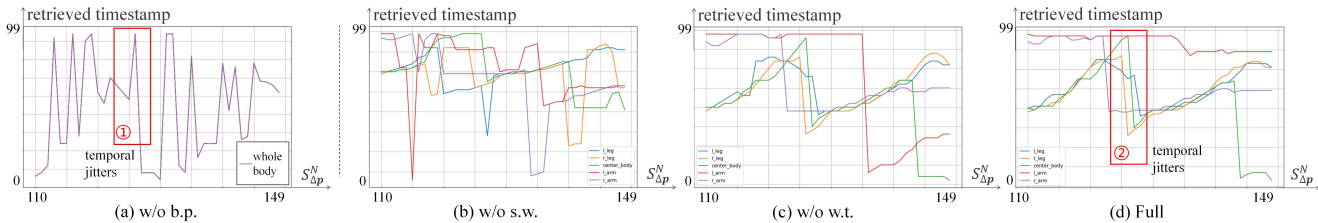


Figure 7. Ablations on design of retrieving algorithm. We show (retrieved timestamps)-(delta pose sequence) curve.

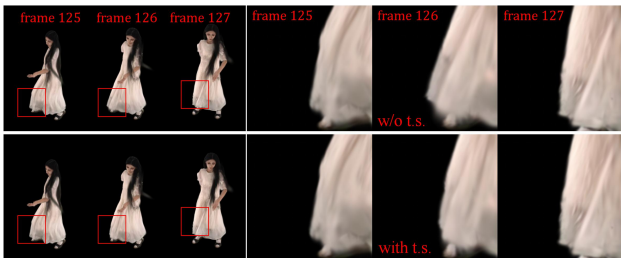


Figure 8. Without smoothing temporal jitters (the first row), the appearance exhibits a drastic change at frame 126, whereas the smoothness of temporal jitters ensures a more seamless animation of the driven avatar (second row).

### 5.5. Out-of-distribution Animation

In Fig. 9, we further demonstrate the animation under completely out-of-distribution poses. Since no similar motions were observed during training, this animation is particularly challenging.

### 6. Limitations and Conclusion

**Limitations.** Although our method can recover high-fidelity human appearance, it relies on multi-view video as inputs. This imposes higher requirements on the capturing equipment, necessitating multiple synchronized cameras covering various viewpoints. Research on recovering human avatars from monocular videos could be a future work, which remains highly challenging. Many works [21, 55, 70] claim to achieve monocular recovery, but they often require videos where the actor fully exposes all body parts (both front and back) or rely on diffusion-based completion to handle unseen views. In the supplemental materials, we include a comparison with monocular methods to validate two key points. First, existing monocular methods degrade significantly on challenging monocular videos. Second, our method still achieves comparable performance on simpler



Figure 9. Animation of human assets under extreme out-of-distribution novel poses.

monocular videos.

**Conclusion.** In this paper, we introduce  $R^3$ -Avatar, a temporal codebook-based framework that effectively addresses the long-standing challenge of balancing high-fidelity rendering and animatability in human avatar reconstruction. By adopting a “record-retrieve-reconstruct” strategy, our method ensures high-quality novel-view rendering while mitigating degradation in novel-pose animation. Specifically, we leverage disambiguating timestamps to encode temporal appearance variations in a codebook and retrieve the most relevant timestamps based on body-part-level pose similarity, enabling robust generalization to unseen poses. Extensive experiments demonstrate that  $R^3$ -Avatar outperforms state-of-the-art video-based human avatar reconstruction approaches, particularly in extreme scenarios with few training poses and complex clothing. Our work aims to inspire advancements in human avatar reconstruction, encouraging further exploration into complex clothing representations, which holds significant potential for broader applications in immersive 3D environments such as AR and VR.



## References

- [1] Badour AlBahar, Shunsuke Saito, Hung-Yu Tseng, Changil Kim, Johannes Kopf, and Jia-Bin Huang. Single-image 3D Human Digitization with Shape-guided Diffusion. In *SIG-GRAPH Asia 2023 Conference Papers*, pages 1–11, 2023. 2
- [2] Thimeo Alldieck, Marcus Magnor, Weipeng Xu, Christian Theobalt, and Gerard Pons-Moll. Video Based Reconstruction of 3D People Models. In *Proceedings of the IEEE Conference on Computer Vision and Pattern Recognition*, pages 8387–8397, 2018. 2
- [3] Thimeo Alldieck, Mihai Zanfir, and Cristian Sminchisescu. Photorealistic Monocular 3D Reconstruction of Humans Wearing Clothing. In *Proceedings of the IEEE/CVF Conference on Computer Vision and Pattern Recognition*, pages 1506–1515, 2022. 2
- [4] Andrés Casado-Elvira, Marc Comino Trinidad, and Dan Casas. Pergamo: Personalized 3D Garments from Monocular Video. In *Computer Graphics Forum*, pages 293–304. Wiley Online Library, 2022. 2
- [5] Jinnan Chen, Chen Li, Jianfeng Zhang, Lingting Zhu, Buzhen Huang, Hanlin Chen, and Gim Hee Lee. Generalizable Human Gaussians from Single-View Image. *arXiv preprint arXiv:2406.06050*, 2024. 2
- [6] Yutong Chen, Yifan Zhan, Zhihang Zhong, Wei Wang, Xiao Sun, Yu Qiao, and Yinqiang Zheng. Within the Dynamic Context: Inertia-aware 3D Human Modeling with Pose Sequence. *arXiv preprint arXiv:2403.19160*, 2024. 1, 2, 5, 6, 7, 14
- [7] Wei Cheng, Ruixiang Chen, Siming Fan, Wanqi Yin, Keyu Chen, Zhongang Cai, Jingbo Wang, Yang Gao, Zhengming Yu, Zhengyu Lin, et al. DNA-Rendering: A Diverse Neural Actor Repository for High-fidelity Human-centric Rendering. In *Proceedings of the IEEE/CVF International Conference on Computer Vision*, pages 19982–19993, 2023. 2, 5, 6, 7, 14, 16
- [8] Patrick Esser, Robin Rombach, and Bjorn Ommer. Taming Transformers for High-resolution Image Synthesis. In *Proceedings of the IEEE/CVF conference on computer vision and pattern recognition*, pages 12873–12883, 2021. 3
- [9] Sara Fridovich-Keil, Giacomo Meanti, Frederik Rahbæk Warburg, Benjamin Recht, and Angjoo Kanazawa. K-planes: Explicit Radiance Fields in Space, Time, and Appearance. In *Proceedings of the IEEE/CVF Conference on Computer Vision and Pattern Recognition*, pages 12479–12488, 2023. 3, 14
- [10] Chen Geng, Sida Peng, Zhen Xu, Hujun Bao, and Xiaowei Zhou. Learning Neural Volumetric Representations of Dynamic Humans in Minutes. In *CVPR*, 2023. 2
- [11] Chen Guo, Xu Chen, Jie Song, and Otmar Hilliges. Human Performance Capture from Monocular Video in the Wild. In *2021 International Conference on 3D Vision (3DV)*, pages 889–898. IEEE, 2021. 2
- [12] Chen Guo, Tianjian Jiang, Xu Chen, Jie Song, and Otmar Hilliges. Vid2avatar: 3D Avatar Reconstruction from Videos in the Wild via Self-supervised Scene Decomposition. In *Proceedings of the IEEE/CVF Conference on Computer Vision and Pattern Recognition*, pages 12858–12868, 2023. 2
- [13] Chen Guo, Tianjian Jiang, Manuel Kaufmann, Chengwei Zheng, Julien Valentin, Jie Song, and Otmar Hilliges. ReLoo: Reconstructing Humans Dressed in Loose Garments from Monocular Video in the Wild. *arXiv preprint arXiv:2409.15269*, 2024. 3
- [14] Marc Habermann, Weipeng Xu, Michael Zollhofer, Gerard Pons-Moll, and Christian Theobalt. Livecap: Real-time Human Performance Capture from Monocular Video. *ACM Transactions On Graphics (TOG)*, 38(2):1–17, 2019. 2
- [15] Marc Habermann, Weipeng Xu, Michael Zollhofer, Gerard Pons-Moll, and Christian Theobalt. Deepcap: Monocular Human Performance Capture using Weak Supervision. In *Proceedings of the IEEE/CVF Conference on Computer Vision and Pattern Recognition*, pages 5052–5063, 2020. 2
- [16] Tong He, John Collomosse, Hailin Jin, and Stefano Soatto. Geo-pifu: Geometry and Pixel Aligned Implicit Functions for Single-view Human Reconstruction. *Advances in Neural Information Processing Systems*, 33:9276–9287, 2020. 2
- [17] Tong He, Yuanlu Xu, Shunsuke Saito, Stefano Soatto, and Tony Tung. Arch++: animation-ready Clothed Human Reconstruction Revisited. In *Proceedings of the IEEE/CVF international conference on computer vision*, pages 11046–11056, 2021. 2
- [18] Martin Heusel, Hubert Ramsauer, Thomas Unterthiner, Bernhard Nessler, and Sepp Hochreiter. GANs Trained by a Two Time-scale Update Rule Converge to a Local Nash Equilibrium. *Advances in neural information processing systems*, 30, 2017. 5
- [19] I Ho, Jie Song, Otmar Hilliges, et al. Sith: Single-view Textured Human Reconstruction with Image-conditioned Diffusion. In *Proceedings of the IEEE/CVF Conference on Computer Vision and Pattern Recognition*, pages 538–549, 2024. 2
- [20] Liangxiao Hu, Hongwen Zhang, Yuxiang Zhang, Boyao Zhou, Boning Liu, Shengping Zhang, and Liqiang Nie. Gaussianavatar: Towards Realistic Human Avatar Modeling from a Single Video via Animatable 3D Gaussians. In *Proceedings of the IEEE/CVF Conference on Computer Vision and Pattern Recognition*, pages 634–644, 2024. 2, 4
- [21] Shoukang Hu, Tao Hu, and Ziwei Liu. Gauhuman: Articulated Gaussian Splatting from Monocular Human Videos. In *Proceedings of the IEEE/CVF Conference on Computer Vision and Pattern Recognition*, pages 20418–20431, 2024. 1, 2, 8, 13
- [22] Yangyi Huang, Hongwei Yi, Yuliang Xiu, Tingting Liao, Jiaxiang Tang, Deng Cai, and Justus Thies. Tech: Text-guided Reconstruction of Lifelike Clothed Humans. In *2024 International Conference on 3D Vision (3DV)*, pages 1531–1542. IEEE, 2024. 2
- [23] Zeng Huang, Yuanlu Xu, Christoph Lassner, Hao Li, and Tony Tung. Arch: Animatable Reconstruction of Clothed Humans. In *Proceedings of the IEEE/CVF Conference on Computer Vision and Pattern Recognition*, pages 3093–3102, 2020. 2
- [24] Mustafa Işık, Martin Rünz, Markos Georgopoulos, Taras Khakhulin, Jonathan Starck, Lourdes Agapito, and Matthias Nießner. Humanrf: High-fidelity Neural Radiance Fields for

- Humans in Motion. *ACM Transactions on Graphics (TOG)*, 42(4):1–12, 2023. 2
- [25] Rohit Jena, Ganesh Subramanian Iyer, Siddharth Choudhary, Brandon Smith, Pratik Chaudhari, and James Gee. Splatarmor: Articulated Gaussian Splatting for Animatable Humans from Monocular RGB Videos. *arXiv preprint arXiv:2311.10812*, 2023. 2
- [26] Boyi Jiang, Yang Hong, Hujun Bao, and Juyong Zhang. Self-recon: Self Reconstruction Your Digital Avatar from Monocular Video. In *Proceedings of the IEEE/CVF Conference on Computer Vision and Pattern Recognition*, pages 5605–5615, 2022. 2
- [27] Wei Jiang, Kwang Moo Yi, Golnoosh Samei, Oncel Tuzel, and Anurag Ranjan. Neuman: Neural Human Radiance Field from a Single Video. In *European Conference on Computer Vision*, pages 402–418. Springer, 2022. 2
- [28] Yuheng Jiang, Zhehao Shen, Yu Hong, Chengcheng Guo, Yize Wu, Yingliang Zhang, Jingyi Yu, and Lan Xu. Robust Dual Gaussian Splatting for Immersive Human-centric Volumetric Videos. *ACM Transactions on Graphics (TOG)*, 43(6):1–15, 2024. 1, 2, 13
- [29] Yuheng Jiang, Zhehao Shen, Penghao Wang, Zhuo Su, Yu Hong, Yingliang Zhang, Jingyi Yu, and Lan Xu. Hifi4g: High-fidelity Human Performance Rendering via Compact Gaussian Splatting. In *Proceedings of the IEEE/CVF conference on computer vision and pattern recognition*, pages 19734–19745, 2024. 1, 2, 5, 7, 13
- [30] Younghyun Jo and Seon Joo Kim. Practical Single-image Super-resolution Using Look-up Table. In *Proceedings of the IEEE/CVF Conference on Computer Vision and Pattern Recognition*, pages 691–700, 2021. 3
- [31] HyunJun Jung, Nikolas Brasch, Jifei Song, Eduardo Perez-Pellitero, Yiren Zhou, Zhihao Li, Nassir Navab, and Benjamin Busam. Deformable 3D Gaussian Splatting for Animatable Human Avatars. *arXiv preprint arXiv:2312.15059*, 2023. 2
- [32] Bernhard Kerbl, Georgios Kopanas, Thomas Leimkühler, and George Drettakis. 3D Gaussian Splatting for Real-Time Radiance Field Rendering. *ACM Transactions on Graphics*, 42(4), 2023. 1, 2, 3, 4, 6
- [33] Jaehyeok Kim, Dongyoon Wee, and Dan Xu. Motion-oriented Compositional Neural Radiance Fields for Monocular Dynamic Human Modeling. In *European Conference on Computer Vision*, pages 476–493. Springer, 2024. 2
- [34] Muhammed Kocabas, Jen-Hao Rick Chang, James Gabriel, Oncel Tuzel, and Anurag Ranjan. Hugs: Human Gaussian Splats. In *Proceedings of the IEEE/CVF conference on computer vision and pattern recognition*, pages 505–515, 2024. 2, 4
- [35] Jiahui Lei, Yufu Wang, Georgios Pavlakos, Lingjie Liu, and Kostas Daniilidis. Gart: Gaussian Articulated Template Models. In *Proceedings of the IEEE/CVF Conference on Computer Vision and Pattern Recognition*, pages 19876–19887, 2024. 1, 2, 5, 6, 7, 14, 16
- [36] Mingwei Li, Jiachen Tao, Zongxin Yang, and Yi Yang. Human101: Training 100+ fps Human Gaussians in 100s from 1 View. *arXiv preprint arXiv:2312.15258*, 2023. 2
- [37] Ruilong Li, Julian Tanke, Minh Vo, Michael Zollhofer, Jürgen Gall, Angjoo Kanazawa, and Christoph Lassner. TAVA: Template-free Animatable Volumetric Actors. 2022. 2
- [38] Xiaoming Li, Chaofeng Chen, Shangchen Zhou, Xianhui Lin, Wangmeng Zuo, and Lei Zhang. Blind Face Restoration via Deep Multi-scale Component Dictionaries. In *European conference on computer vision*, pages 399–415. Springer, 2020. 3
- [39] Zhe Li, Zerong Zheng, Yuxiao Liu, Boyao Zhou, and Yebin Liu. Posevocab: Learning Joint-structured Pose Embeddings for Human Avatar Modeling. In *ACM SIGGRAPH 2023 Conference Proceedings*, pages 1–11, 2023. 1, 2
- [40] Zhe Li, Zerong Zheng, Lizhen Wang, and Yebin Liu. Animatable Gaussians: Learning Pose-dependent Gaussian Maps for High-fidelity Human Avatar Modeling. In *Proceedings of the IEEE/CVF Conference on Computer Vision and Pattern Recognition*, pages 19711–19722, 2024. 1, 2
- [41] Haotong Lin, Sida Peng, Zhen Xu, Tao Xie, Xingyi He, Hujun Bao, and Xiaowei Zhou. High-Fidelity and Real-Time Novel View Synthesis for Dynamic Scenes. In *SIGGRAPH Asia Conference Proceedings*, 2023. 1, 2, 5, 13
- [42] Lingjie Liu, Marc Habermann, Viktor Rudnev, Kripasindhu Sarkar, Jiatao Gu, and Christian Theobalt. Neural actor: Neural Free-view Synthesis of Human Actors with Pose Control. *ACM transactions on graphics (TOG)*, 40(6):1–16, 2021. 2
- [43] Xinqi Liu, Chenming Wu, Jialun Liu, Xing Liu, Chen Zhao, Haocheng Feng, Errui Ding, and Jingdong Wang. Gva: Reconstructing Vivid 3D Gaussian Avatars from Monocular Videos. *CoRR*, 2024. 2
- [44] Matthew Loper, Naureen Mahmood, Javier Romero, Gerard Pons-Moll, and Michael J Black. SMPL: A Skinned Multi-Person Linear Model. *ACM Transactions on Graphics*, 34(6), 2015. 2, 3, 13
- [45] Ben Mildenhall, Pratul P Srinivasan, Matthew Tancik, Jonathan T Barron, Ravi Ramamoorthi, and Ren Ng. NeRF: Representing Scenes as Neural Radiance Fields for View Synthesis. In *European Conference on Computer Vision*, pages 405–421, 2020. 1, 2, 6
- [46] Gyeongsik Moon, Hyeongjin Nam, Takaaki Shiratori, and Kyoung Mu Lee. 3d Clothed Human Reconstruction in the Wild. In *European conference on computer vision*, pages 184–200. Springer, 2022. 2
- [47] Gyeongsik Moon, Takaaki Shiratori, and Shunsuke Saito. Expressive Whole-body 3D Gaussian Avatar. In *European Conference on Computer Vision*, pages 19–35. Springer, 2024. 2, 4
- [48] Panwang Pan, Zhuo Su, Chenguo Lin, Zhen Fan, Yongjie Zhang, Zeming Li, Tingting Shen, Yadong Mu, and Yebin Liu. Humansplat: Generalizable Single-image Human Gaussian Splatting with Structure Priors. *Advances in Neural Information Processing Systems*, 37:74383–74410, 2025. 2
- [49] Haokai Pang, Heming Zhu, Adam Kortylewski, Christian Theobalt, and Marc Habermann. Ash: Animatable Gaussian Splats for Efficient and Photoreal Human Rendering. In *Proceedings of the IEEE/CVF Conference on Computer Vision and Pattern Recognition*, pages 1165–1175, 2024. 1, 2

- [50] Pramish Paudel, Anubhav Khanal, Danda Pani Paudel, Jyoti Tandukar, and Ajad Chhatkuli. ihuman: Instant animatable digital humans from monocular videos. In *European Conference on Computer Vision*, pages 304–323. Springer, 2024. **2**
- [51] Georgios Pavlakos, Vasileios Choutas, Nima Ghorbani, Timo Bolkart, Ahmed A. A. Osman, Dimitrios Tzionas, and Michael J. Black. Expressive Body Capture: 3D Hands, Face, and Body from a Single Image. In *Proceedings IEEE Conf. on Computer Vision and Pattern Recognition (CVPR)*, pages 10975–10985, 2019. **2, 3, 13**
- [52] Sida Peng, Yuanqing Zhang, Yinghao Xu, Qianqian Wang, Qing Shuai, Hujun Bao, and Xiaowei Zhou. Neural Body: Implicit Neural Representations with Structured Latent Codes for Novel View Synthesis of Dynamic Humans. In *CVPR*, 2021. **2, 5, 6, 13, 14**
- [53] Sida Peng, Chen Geng, Yuanqing Zhang, Yinghao Xu, Qianqian Wang, Qing Shuai, Xiaowei Zhou, and Hujun Bao. Implicit Neural Representations with Structured Latent Codes for Human Body Modeling. *IEEE Transactions on Pattern Analysis and Machine Intelligence*, 2023. **1**
- [54] Sida Peng, Zhen Xu, Junting Dong, Qianqian Wang, Shangzhan Zhang, Qing Shuai, Hujun Bao, and Xiaowei Zhou. Animatable Implicit Neural Representations for Creating Realistic Avatars from Videos. *TPAMI*, 2024. **2**
- [55] Zhiyin Qian, Shaofei Wang, Marko Mihajlovic, Andreas Geiger, and Siyu Tang. 3dgs-avatar: Animatable Avatars via Deformable 3d Gaussian Splatting. In *Proceedings of the IEEE/CVF Conference on Computer Vision and Pattern Recognition*, pages 5020–5030, 2024. **1, 2, 8**
- [56] Javier Romero, Dimitrios Tzionas, and Michael J. Black. Embodied Hands: Modeling and Capturing Hands and Bodies Together. *ACM Transactions on Graphics, (Proc. SIGGRAPH Asia)*, 36(6), 2017. **3**
- [57] Shunsuke Saito, Zeng Huang, Ryota Natsume, Shigeo Morishima, Angjoo Kanazawa, and Hao Li. Pifu: Pixel-aligned Implicit Function for High-resolution Clothed Human Digitization. In *Proceedings of the IEEE/CVF international conference on computer vision*, pages 2304–2314, 2019. **2**
- [58] Shunsuke Saito, Tomas Simon, Jason Saragih, and Hanbyul Joo. Pifuhd: Multi-level Pixel-aligned Implicit Function for High-resolution 3D Human Digitization. In *Proceedings of the IEEE/CVF conference on computer vision and pattern recognition*, pages 84–93, 2020. **2**
- [59] Zhijing Shao, Zhaolong Wang, Zhuang Li, Duotun Wang, Xiangru Lin, Yu Zhang, Mingming Fan, and Zeyu Wang. Splattingavatar: Realistic Real-time Human Avatars with Mesh-embedded Gaussian Splatting. In *Proceedings of the IEEE/CVF Conference on Computer Vision and Pattern Recognition*, pages 1606–1616, 2024. **2, 5, 6, 7, 14**
- [60] Shih-Yang Su, Frank Yu, Michael Zollhöfer, and Helge Rhodin. A-nerf: Articulated Neural Radiance Fields for Learning Human Shape, Appearance, and Pose. *Advances in neural information processing systems*, 34:12278–12291, 2021. **2**
- [61] Shih-Yang Su, Timur Bagautdinov, and Helge Rhodin. Danbo: Disentangled Articulated Neural Body Representations via Graph Neural Networks. In *European Conference on Computer Vision*, pages 107–124. Springer, 2022.
- [62] Shih-Yang Su, Timur Bagautdinov, and Helge Rhodin. Npc: Neural Point Characters from Video. In *Proceedings of the IEEE/CVF International Conference on Computer Vision*, pages 14795–14805, 2023. **2**
- [63] Adam Sun, Tiange Xiang, Scott Delp, Li Fei-Fei, and Ehsan Adeli. OccFusion: Rendering Occluded Humans with Generative Diffusion Priors. *arXiv preprint arXiv:2407.00316*, 2024. **2**
- [64] David Svitov, Dmitrii Gudkov, Renat Bashirov, and Victor Lempitsky. Dinar: Diffusion Inpainting of Neural Textures for One-shot Human Avatars. In *Proceedings of the IEEE/CVF International Conference on Computer Vision*, pages 7062–7072, 2023. **2, 3**
- [65] Jeff Tan, Donglai Xiang, Shubham Tulsiani, Deva Ramanan, and Gengshan Yang. DressRecon: Freeform 4D Human Reconstruction from Monocular Video. *arXiv preprint arXiv:2409.20563*, 2024. **3, 5, 13, 14**
- [66] Matthew Tancik, Pratul Srinivasan, Ben Mildenhall, Sara Fridovich-Keil, Nithin Raghavan, Utkarsh Singhal, Ravi Ramamoorthi, Jonathan Barron, and Ren Ng. Fourier Features Let Networks Learn High Frequency Functions in Low Dimensional Domains. *Advances in neural information processing systems*, 33:7537–7547, 2020. **6**
- [67] Aaron Van Den Oord, Oriol Vinyals, et al. Neural Discrete Representation Learning. *Advances in neural information processing systems*, 30, 2017. **3**
- [68] Shaofei Wang, Katja Schwarz, Andreas Geiger, and Siyu Tang. Arah: Animatable volume rendering of articulated human sdf. In *European conference on computer vision*, pages 1–19. Springer, 2022. **1, 2**
- [69] Zhou Wang, Alan C Bovik, Hamid R Sheikh, and Eero P Simoncelli. Image Quality Assessment: from Error Visibility to Structural Similarity. *IEEE transactions on image processing*, 13(4):600–612, 2004. **5**
- [70] Zilong Wang, Zhiyang Dou, Yuan Liu, Cheng Lin, Xiao Dong, Yunhui Guo, Chenxu Zhang, Xin Li, Wenping Wang, and Xiaohu Guo. WonderHuman: Hallucinating Unseen Parts in Dynamic 3D Human Reconstruction. *arXiv preprint arXiv:2502.01045*, 2025. **2, 4, 5, 8**
- [71] Chung-Yi Weng, Brian Curless, Pratul P Srinivasan, Jonathan T Barron, and Ira Kemelmacher-Shlizerman. Humannerf: Free-viewpoint Rendering of Moving People from Monocular Video. In *Proceedings of the IEEE/CVF conference on computer vision and pattern Recognition*, pages 16210–16220, 2022. **1, 2**
- [72] Zhangyang Xiong, Chenghong Li, Kenkun Liu, Hongjie Liao, Jianqiao Hu, Junyi Zhu, Shuliang Ning, Lingteng Qiu, Chongjie Wang, Shijie Wang, et al. MVHumanNet: A Large-scale Dataset of Multi-view Daily Dressing Human Captures. In *Proceedings of the IEEE/CVF Conference on Computer Vision and Pattern Recognition*, pages 19801–19811, 2024. **2, 5, 6**
- [73] Yuliang Xiu, Jinlong Yang, Dimitrios Tzionas, and Michael J Black. Icon: Implicit Clothed Humans Obtained from Normals. In *2022 IEEE/CVF Conference on Computer Vi-*

- sion and Pattern Recognition (CVPR)*, pages 13286–13296. IEEE, 2022. [2](#)
- [74] Yuliang Xiu, Jinlong Yang, Xu Cao, Dimitrios Tzionas, and Michael J Black. Econ: Explicit Clothed Humans Optimized via Normal Integration. In *Proceedings of the IEEE/CVF conference on computer vision and pattern recognition*, pages 512–523, 2023. [2](#)
- [75] Weipeng Xu, Avishek Chatterjee, Michael Zollhöfer, Helge Rhodin, Dushyant Mehta, Hans-Peter Seidel, and Christian Theobalt. Monoperfcap: Human Performance Capture from Monocular Video. *ACM Transactions on Graphics (ToG)*, 37(2):1–15, 2018. [2](#)
- [76] Wangze Xu, Yifan Zhan, Zhihang Zhong, and Xiao Sun. GAST: Sequential Gaussian Avatars with Hierarchical Spatio-temporal Context. *arXiv preprint arXiv:2411.16768*, 2024. [2](#)
- [77] Zhen Xu, Sida Peng, Haotong Lin, Guangzhao He, Jiaming Sun, Yujun Shen, Hujun Bao, and Xiaowei Zhou. 4K4D: Real-time 4D View Synthesis at 4K Resolution. In *Proceedings of the IEEE/CVF conference on computer vision and pattern recognition*, pages 20029–20040, 2024. [1](#), [2](#), [13](#)
- [78] Zeyu Yang, Hongye Yang, Zijie Pan, and Li Zhang. Real-time Photorealistic Dynamic Scene Representation and Rendering with 4D Gaussian Splatting. *arXiv preprint arXiv:2310.10642*, 2023. [5](#), [6](#), [14](#)
- [79] Junhui Yin, Wei Yin, Hao Chen, Xuqian Ren, Zhanyu Ma, Jun Guo, and Yifan Liu. HumanRecon: Neural Reconstruction of Dynamic Human Using Geometric Cues and Physical Priors. *arXiv preprint arXiv:2311.15171*, 2023. [2](#)
- [80] Zhengming Yu, Wei Cheng, Xian Liu, Wayne Wu, and Kwan-Yee Lin. MonoHuman: Animatable Human Neural Field from Monocular Video. In *Proceedings of the IEEE/CVF Conference on Computer Vision and Pattern Recognition*, pages 16943–16953, 2023. [2](#)
- [81] Jingbo Zhang, Xiaoyu Li, Qi Zhang, Yanpei Cao, Ying Shan, and Jing Liao. Humanref: Single Image to 3D Human Generation via Reference-guided Diffusion. In *Proceedings of the IEEE/CVF Conference on Computer Vision and Pattern Recognition*, pages 1844–1854, 2024. [2](#)
- [82] Richard Zhang, Phillip Isola, Alexei A Efros, Eli Shechtman, and Oliver Wang. The Unreasonable Effectiveness of Deep Features as a Perceptual Metric. In *Proceedings of the IEEE conference on computer vision and pattern recognition*, pages 586–595, 2018. [5](#)
- [83] Hao Zhao, Jinsong Zhang, Yu-Kun Lai, Zerong Zheng, Yingdi Xie, Yebin Liu, and Kun Li. High-fidelity Human Avatars from a Single RGB Camera. In *Proceedings of the IEEE/CVF Conference on Computer Vision and Pattern Recognition*, pages 15904–15913, 2022. [2](#)
- [84] Shunyuan Zheng, Boyao Zhou, Ruizhi Shao, Boning Liu, Shengping Zhang, Liqiang Nie, and Yebin Liu. Gps-gaussian: Generalizable Pixel-wise 3D Gaussian Splatting for Real-time Human Novel View Synthesis. In *Proceedings of the IEEE/CVF Conference on Computer Vision and Pattern Recognition*, pages 19680–19690, 2024. [1](#), [2](#), [13](#), [14](#)
- [85] Zerong Zheng, Tao Yu, Yebin Liu, and Qionghai Dai. Pamir: Parametric Model-conditioned Implicit Representation for Image-based Human Reconstruction. *IEEE transactions on pattern analysis and machine intelligence*, 44(6):3170–3184, 2021. [2](#)
- [86] Zerong Zheng, Han Huang, Tao Yu, Hongwen Zhang, Yandong Guo, and Yebin Liu. Structured Local Radiance Fields for Human Avatar Modeling. In *Proceedings of the IEEE/CVF Conference on Computer Vision and Pattern Recognition*, pages 15893–15903, 2022. [2](#)
- [87] Boyao Zhou, Shunyuan Zheng, Hanzhang Tu, Ruizhi Shao, Boning Liu, Shengping Zhang, Liqiang Nie, and Yebin Liu. GPS-Gaussian+: Generalizable Pixel-wise 3D Gaussian Splatting for Real-Time Human-Scene Rendering from Sparse Views. *arXiv preprint arXiv:2411.11363*, 2024. [1](#), [2](#), [5](#), [13](#)
- [88] Shangchen Zhou, Kelvin Chan, Chongyi Li, and Chen Change Loy. Towards Robust Blind Face Restoration with Codebook Lookup Transformer. *Advances in Neural Information Processing Systems*, 35:30599–30611, 2022. [3](#)
- [89] Zi-Xin Zou, Zhipeng Yu, Yuan-Chen Guo, Yanguang Li, Ding Liang, Yan-Pei Cao, and Song-Hai Zhang. Triplane Meets Gaussian Splatting: Fast and Generalizable Single-view 3D Reconstruction with Transformers. In *Proceedings of the IEEE/CVF conference on computer vision and pattern recognition*, pages 10324–10335, 2024. [2](#), [4](#)

## A. Supplemental Material

### A.1. Comparison under Monocular Setting

Our method exhibits degraded performance on monocular videos. The main reason is that temporal encoding allows different frames to have varying appearances. When multi-view constraints are insufficient, the degrees of freedom for unseen views increase. However, we point out that some methods [21, 65] claiming to recover the human body from monocular videos rely on highly constrained input, requiring the person to fully expose their body parts (both front and back) to the camera.

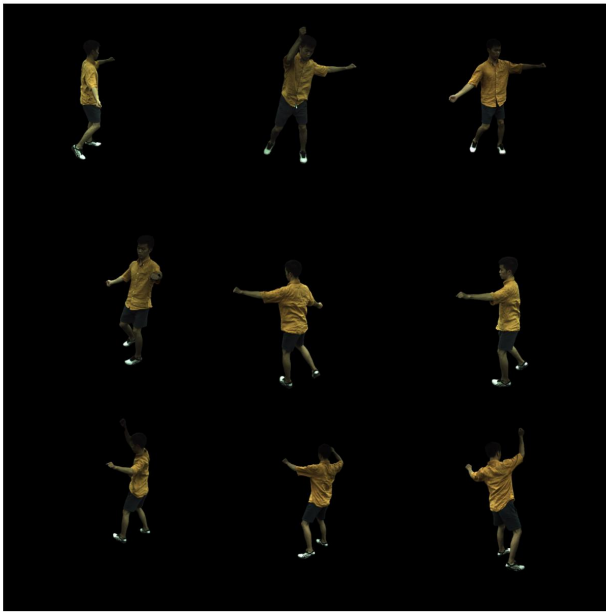


Figure 10. A monocular video example from the highly constrained ZJU\_MoCap dataset. The person is fully exposed to the camera.

In Fig. 10, we show an example of ZJU\_MoCap dataset [52] to illustrate this strict capturing. And in the cases shown in Tab. 4 and Fig. 11 (ZJU\_MoCap dataset trained from monocular video), our method performs slightly worse than the monocular-based DressRecon [65], which lacks animatability.

We further apply monocular methods for reconstruction on unconstrained capture data. As shown in Fig. 12, the reconstruction quality significantly deteriorates, indicating that these methods are not capable of perfectly handling all monocular data. Our multi-view setting circumvents these challenges, allowing us to focus on human rendering and animation. That said, recovering human bodies from imperfectly captured monocular videos remains a challenge.

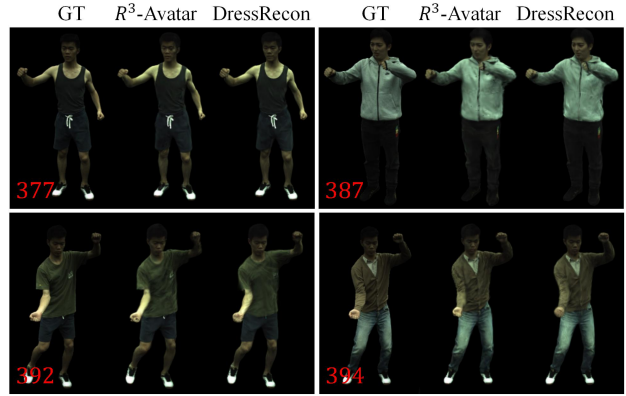


Figure 11. Qualitative comparison of our method and DressRecon on the ZJU\_MoCap dataset [52].

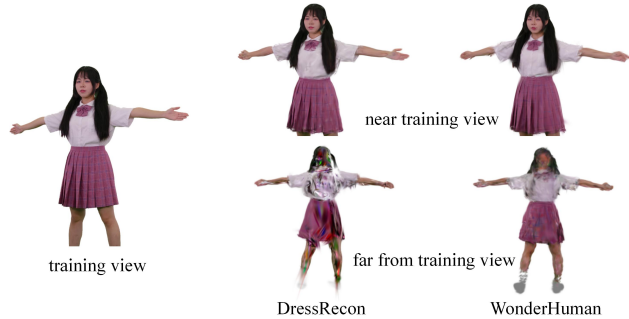


Figure 12. Qualitative results of DressRecon and WonderHuman on unconstrained capture data.

### A.2. Comparison with Rendering-based Methods

Rendering-based human avatars focus on recovering 3D human bodies from images or videos without the requirement for animation. A class of methods [28, 29, 41, 77, 84, 87] employs multi-view image-based rendering strategies, using reference views to enhance the rendering quality from source views. We compare our method with GPS-Gaussian [84], one of the cutting-edge rendering-based method. Fig. 15 and Tab. 5 reveal that although GPS-Gaussian does not require per-scene training, it falls short of our method in novel-view rendering quality and lacks the ability to animate.

### A.3. Partitioning of Human Body

In Sec. 4.3. (main text), we propose a body partitioning strategy to retrieve timestamps for different body parts separately. Our partitioning is based on the observed coupling of body motion. For example, hands and legs typically do not affect the same region and are therefore separated, whereas the hip and waist are usually correlated and thus should be grouped together. In Fig. 13 we display the results of partitioning on both SMPL [44] and SMPL-X [51].

Method	377			386			387		
	PSNR $\uparrow$	SSIM $\uparrow$	LPIPS $\downarrow$	PSNR $\uparrow$	SSIM $\uparrow$	LPIPS $\downarrow$	PSNR $\uparrow$	SSIM $\uparrow$	LPIPS $\downarrow$
DressRecon [65]	<b>31.30</b>	<b>0.971</b>	<b>21.2</b>	31.96	0.963	<b>34.2</b>	27.60	<b>0.952</b>	<b>38.9</b>
$R^3$ -Avatar (ours)	30.82	0.968	30.0	<b>32.41</b>	<b>0.964</b>	40.0	<b>27.79</b>	0.951	46.8
Method	392			393			394		
	PSNR $\uparrow$	SSIM $\uparrow$	LPIPS $\downarrow$	PSNR $\uparrow$	SSIM $\uparrow$	LPIPS $\downarrow$	PSNR $\uparrow$	SSIM $\uparrow$	LPIPS $\downarrow$
DressRecon [65]	<b>31.94</b>	<b>0.964</b>	<b>31.0</b>	<b>29.81</b>	<b>0.956</b>	<b>34.6</b>	31.02	<b>0.958</b>	<b>30.2</b>
$R^3$ -Avatar (ours)	31.92	0.961	39.8	29.40	0.951	44.3	<b>31.06</b>	0.956	39.2

Table 4. Per-scene quantitative comparisons on the monocular ZJU\_MoCap dataset [52].

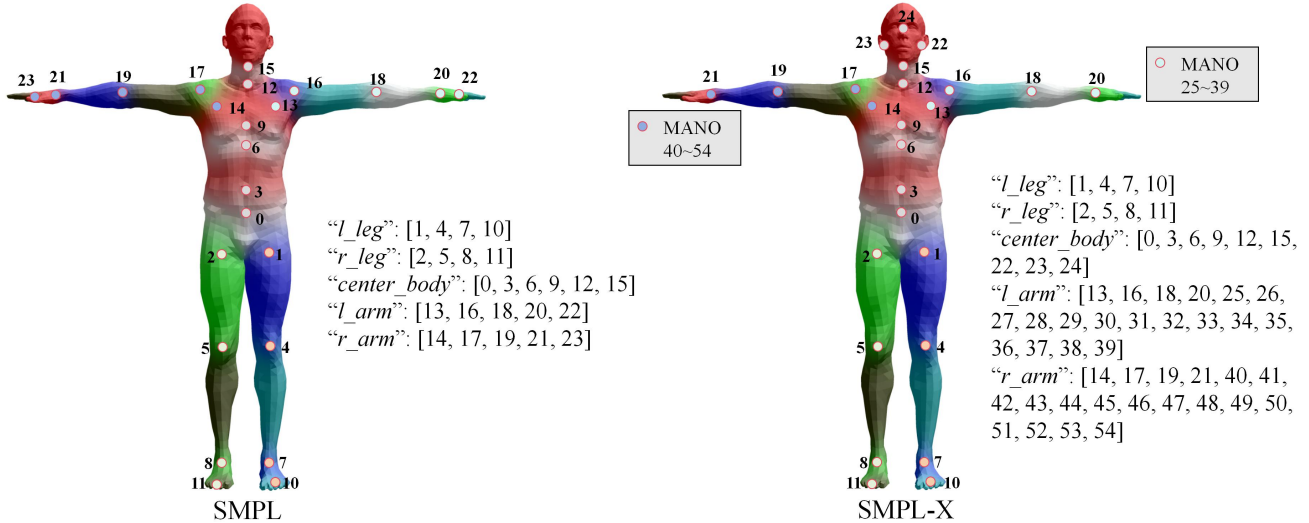


Figure 13. The body partitioning during retrieving on both SMPL (ZJU\_MoCap dataset, Hifi4G dataset) and SMPL-X (DNA-Rendering dataset, MVHumanNet dataset).

	PSNR $\uparrow$	SSIM $\uparrow$	LPIPS $\downarrow$
GPS-Gaussian [84]	31.02	0.970	29.6
$R^3$ -Avatar (ours)	<b>32.43</b>	<b>0.974</b>	<b>25.2</b>

Table 5. Novel-view rendering comparison of our method and GPS-Gaussian on DNA-Rendering dataset [7]. LPIPS is  $1000\times$ .

	4DGS	Dyco	GART	SplattngAvatar	$R^3$ -Avatar (ours)
Training Time	3h	16h	30min	60min	90min
Rendering Speed (FPS)	60+	0.5	60+	50+	60+

Table 6. Average training (till convergence) time and rendering speed on DNA-Rendering dataset [7].

#### A.4. Training and Rendering Efficiency

We train all baselines (4DGS [78], Dyco [6], GART [35], SplattngAvatar [59] and  $R^3$ -Avatar) on a single GeForce RTX3090. Training time and rendering speed on DNA-Rendering dataset [7] are reported in Tab. 6. Our method achieves better rendering and animation quality at a comparable rendering speed compared to GART and SplattngAvatar. Dyco’s training time and inference speed make it challenging to apply in real-time scenarios.

#### A.5. Ablations on Hyperparameters of Recording Phase

For hyperparameters of the spatial encoder, we apply multi-scale planes [9] with 3 different resolutions at  $64^2$ ,  $128^2$ ,  $256^2$ . For hyperparameters of the temporal codebook, we only apply multi-scale encoding on spatial resolutions, keeping the time resolution to be 50. Now we have the biggest plane set ( $\mathbf{P}_{xy}[256 \times 256]$ ,  $\mathbf{P}_{xz}[256 \times 256]$ ,  $\mathbf{P}_{yz}[256 \times 256]$ ,  $\mathbf{P}_{xt}[256 \times 50]$ ,  $\mathbf{P}_{yt}[256 \times 50]$ ,  $\mathbf{P}_{zt}[256 \times 50]$ ), which is displayed in Fig. 14. And the smallest plane set is ( $\mathbf{P}_{xy}[64 \times 64]$ ,  $\mathbf{P}_{xz}[64 \times 64]$ ,  $\mathbf{P}_{yz}[64 \times 64]$ ,  $\mathbf{P}_{xt}[64 \times 50]$ ,  $\mathbf{P}_{yt}[64 \times 50]$ ,  $\mathbf{P}_{zt}[64 \times 50]$ ). The per-plane and per-scale features are multiplied across planes and concatenated across scales. The per-plane and per-scale features ( $\mathbf{f}_{xy}$ ,  $\mathbf{f}_{xz}$ ,  $\mathbf{f}_{yz}$ ,  $\mathbf{f}_{xt}$ ,  $\mathbf{f}_{yt}$ ,  $\mathbf{f}_{zt}$ ) all have dimension 32, so the final encoded feature  $\mathbf{f}$  has dimension 128. For hyperparameters of 4D gaussian decoder and LBS network, we detail the number of layers and the width of the MLP.  $\Phi_{gd}$  has  $D = 2$  and  $W = 256$ .  $\Phi_{lbs}$  has  $D = 4$  and  $W = 128$ .

We conduct additional ablation experiments on hyperparameter settings. First, we explore the impact of selecting different resolutions for the hex-plane encoder. In Tab. 7,

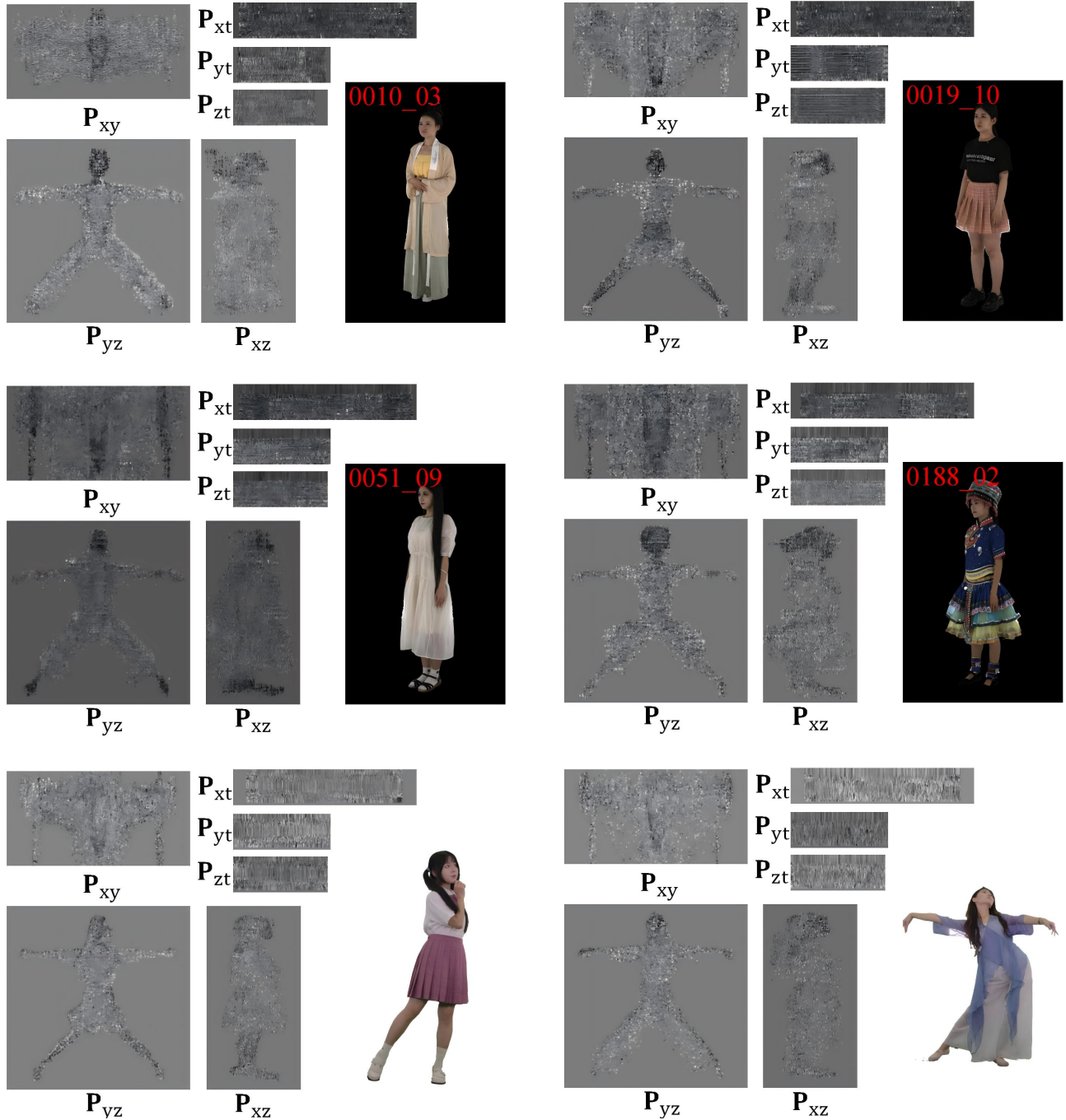


Figure 14. Hex-plane spatio-temporal encoder for different human avatars.

we test with four different spatial resolutions while keeping temporal resolutions to 50 (“level N, Res” means using “N” level of multi-scale planes with max resolution “Res”). We observe a performance improvement with increased resolution, with the marginal gains gradually diminishing. As a trade-off, we select the resolution as 256, striking a balance between minimizing memory consumption and satisfactory

performance.

#### A.6. Ablations on Hyperparameters of Retrieving Phase

For retrieving phase, length of delta pose sequence  $S_{\Delta p}^N$  is 2,  $k$  in  $S_{\text{top}k}$  is set to 20, sliding window size  $W$  is 3.

The “delta pose sequence” provides motion direction

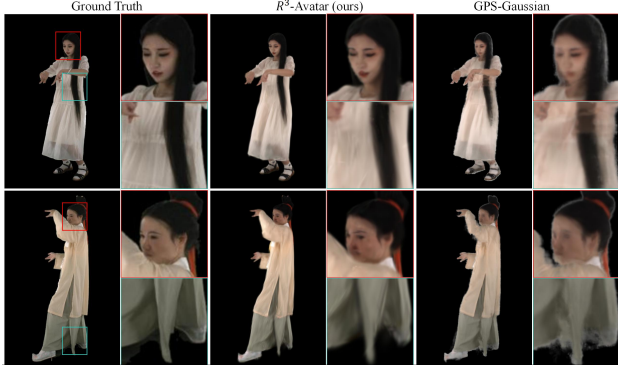


Figure 15. Novel-view rendering comparison of our method and GPS-Gaussian on DNA-Rendering dataset [7].

Resolution	PSNR $\uparrow$	SSIM $\uparrow$	LPIPS $\downarrow$
level 1, 64	29.13	0.957	43.7
level 2, 128	32.01	0.970	27.4
level 3, 256 (ours)	<b>32.43</b>	<b>0.974</b>	<b>25.2</b>
level 4, 512	32.47	0.974	25.0

Table 7. Ablations on the resolution of hex-plane encoder. We show the novel-view rendering results on DNA-Rendering dataset [7]. LPIPS is  $1000\times$ .

during retrieving, facilitating pose matching. However, an excessive length of  $S_{\Delta p}^N$  will reduce matching samples in training sets. We ablate the length of delta pose sequence in Tab. 8.

$\mathcal{S}_{\text{top}k}$  is the set of training poses (or delta pose sequences) ranked by similarity based on their L2 distance to the current novel pose (or delta pose sequence). The sliding window prioritizes poses from this set, considering only those whose timestamps fall within the sliding window relative to the previous novel-pose frames (*e.g.*, if the previous novel pose retrieved timestamp 30, then the timestamps within the sliding window range would be  $[30 - W, 30 + W]$ . Any pose within this range in  $\mathcal{S}_{\text{top}k}$  will be prioritized). If  $k$  is too big, the retrieved pose is less reliable because more low-confidence poses have been included. However, if  $k$  is too small, it is likely that no poses within the sliding window will be found, increasing temporal jitters. As for size of sliding window, a value too small reduces the number of poses falling within the sliding window, leading to temporal jitters, while a value too large diminishes the smoothing effect of the window, as even poses from distant timestamps may fall within the same window. In Tab. 8, we also ablate these two items.

## B. More visual Results

We display more visualization in Fig. 18 (novel-view rendering) and Fig. 17 (novel-pose animating).

Resolution	PSNR $\uparrow$	SSIM $\uparrow$	LPIPS $\downarrow$	FID $\downarrow$
$ S_{\Delta p}^N  = 0$	24.94	0.942	49.9	3.45
$ S_{\Delta p}^N  = 2$ (ours)	<b>25.21</b>	<b>0.945</b>	<b>47.2</b>	<b>3.39</b>
$ S_{\Delta p}^N  = 4$	24.73	0.941	49.7	3.42
$k = 5$	25.09	0.944	48.1	3.43
$k = 20$ (ours)	<b>25.21</b>	<b>0.945</b>	<b>47.2</b>	<b>3.39</b>
$k = 50$	24.92	0.941	48.6	3.44
$W = 1$	25.11	0.944	47.6	3.44
$W = 3$ (ours)	<b>25.21</b>	<b>0.945</b>	<b>47.2</b>	<b>3.39</b>
$W = 5$	25.03	0.942	48.1	3.46

Table 8. Ablations on hyperparameters of retrieving phase. We show the novel-pose animation results on DNA-Rendering dataset [7]. LPIPS is  $1000\times$ .

### B.1. Human in the Scene

Since  $R^3$ -Avatar employs 3DGS-based representation, the reconstructed avatar supports seamless integration with other GS assets, *e.g.*, the scene, and is therefore compatible with conventional rendering pipeline for 3DGS. Fig. 16 presents an example of 3D human avatars integrated into a scene reconstructed by 3DGS.

### B.2. Supplemental Video

We have also attached a supplementary video alongside this PDF file, which consists of novel-view rendering and novel-pose animation, together with visual comparisons with GART [35], one of the current state-of-the-art methods. Since images may not fully convey the effectiveness of human reconstruction, especially for the results of animation, we encourage the readers to watch the supplemental video.





Figure 16. Render the human assets together with the scene.

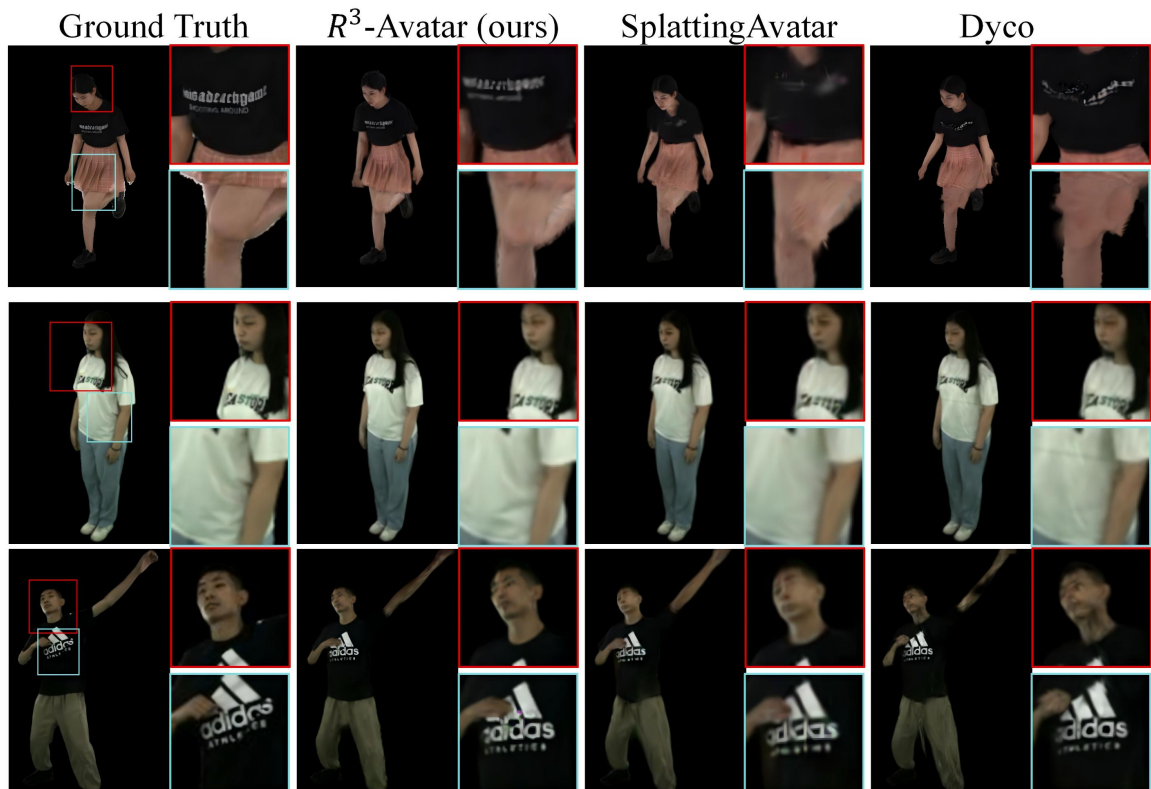


Figure 17. More results of novel-pose animating.

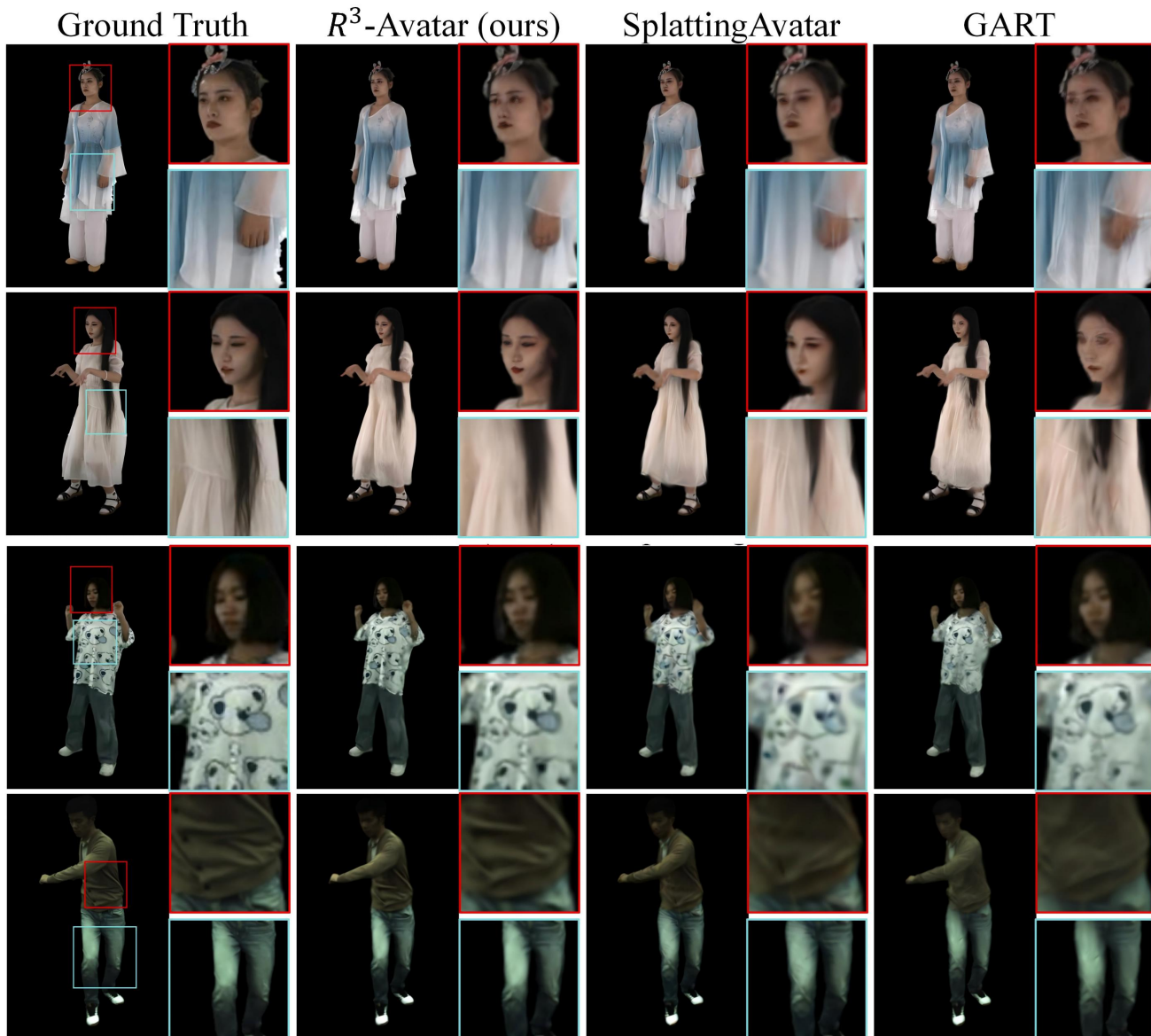


Figure 18. More results of novel-view rendering.